Available online at www.sciencedirect.com
SCIENCE DIRECT
Journal of Solid State Chemistry 179 (2006) 2495–2505
JOURNAL OF SOLID STATE CHEMISTRY
www.elsevier.com/locate/jssc

Local crystal chemistry, structured diffuse scattering and the dielectric properties of $(Bi_{1-x}Y_x)_2(M^{III}Nb^V)O_7$ ($M = Fe^{3+}$, In^{3+}) Bi-pyrochlores

W. Somphon[a], V. Ting[a], Y. Liu[a], R.L. Withers[a,*], Q. Zhou[b], B.J. Kennedy[b]

[a]*Research School of Chemistry, Australian National University, Canberra, ACT 0200, Australia*
[b]*School of Chemistry, Sydney University, Sydney, Australia*

Received 19 December 2005; received in revised form 22 March 2006; accepted 8 April 2006
Available online 10 May 2006

Abstract

Electron diffraction is used to investigate the large amplitude displacive disorder characteristic of the $Bi_2(M^{III}Nb^V)O_7$ Bi-pyrochlores, Bi_2InNbO_7 and Bi_2FeNbO_7, as well as of their *A* site substituted $Bi_{1.5}Y_{0.5}InNbO_7$ and $Bi_{1.5}Y_{0.5}FeNbO_7$ variants. Highly structured diffuse distributions in the form of {110}* sheets of diffuse intensity perpendicular to the six ⟨110⟩ directions of real space along with ⟨111⟩* rods of diffuse intensity perpendicular to the four {111} real space planes are observed. The existence of this structured diffuse scattering is interpreted in terms of large amplitude, *β*-cristobalite-type tetrahedral rotations of the $O'A_2$ tetrahedral framework substructure of the ideal pyrochlore structure type. Bond valence sum calculations are used to understand the local crystal chemistry responsible for such displacive disorder. The frequency-dependent dielectric properties of Bi_2InNbO_7 and Bi_2FeNbO_7 are also investigated along with the effect upon them of *A* site doping with Y.

Keywords: Structured diffuse scattering; Electron diffraction investigation of; Bi-pyrochlores; Displacive disorder therein

1. Introduction

The ever-expanding global market for wireless communication devices provides a strong incentive to search for new, and/or improved, microwave dielectric materials. In particular, dielectric ceramics which have high relative permittivities, low dielectric losses as well as low-temperature coefficients of permittivity are of great interest for use as microwave dielectric resonators, oscillators and filters [1–3]. Materials of this type whose dielectric properties are furthermore tuneable under the action of an applied electric or magnetic field and which can be sintered at relatively low temperatures are of even greater interest [4–6]. Potential applications include use as co-fired multilayer ceramic capacitors (MLCC), tunable filters, phase shifters, electrically steerable antennas, etc. Amongst the limited range of current candidate materials, Bi-based pyrochlore systems, such as, e.g., $Bi_{1.5}ZnNb_{1.5}O_7$ (BZN), $Bi_2(Zn_{2/3}Nb_{4/3})O_7$ and related systems, $Bi_2(M^{III}Nb^V)O_7$, etc. [5–9], show great potential.

Of such Bi-based, $A_2B_2O_7$ or $O'A_2 \cdot B_2O_6$, pyrochlore systems (see Fig. 1), many are known to be strongly displacively disordered, particularly on the $O'A_2$ substructure (see e.g., [10–15] and references contained therein). Indeed, after careful consideration, Vanderah et al. [15] have recently even gone so far as to conclude that "… the occurrence of displacive disorder in the $O'A_2$ network is *required* for the formation of pyrochlore …" in many such Bi-pyrochlore systems. It has frequently been found, for example, that Bi ions when placed on the 16*d* ideal *A* site positions of the pyrochlore structure type exhibit anomalously large atomic displacement parameters (adp's) [10–14]. Indeed the adp's have often been so large that the structure has been found to be rather better modelled by displacing the Bi/*A* site ions perpendicular to the local three-fold O′–Bi–O′ axes by up to ~0.5 Å or so into 96*g* or 96*h* sites (see, e.g., Fig. 1 of [12] and Refs. [10–15]). Formally, the Bi and other *A* site ions are then able to occupy any one of up to 6 equivalent such displacively disordered local positions (see, e.g., Fig. 1 of [12]).

*Corresponding author. Fax: 61 2 6125 0750.
E-mail address: withers@rsc.anu.edu.au (R.L. Withers).

0022-4596/$ - see front matter © 2006 Elsevier Inc. All rights reserved.
doi:10.1016/j.jssc.2006.04.046

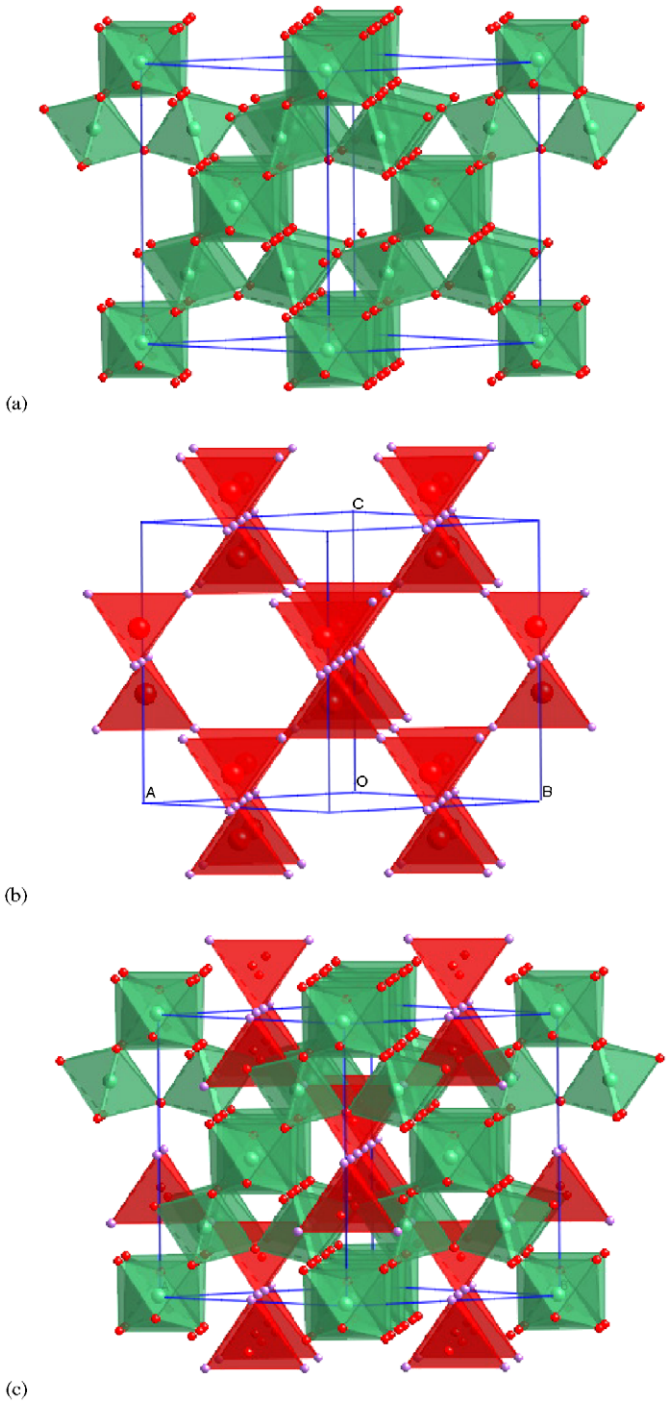

Fig. 1. The (a) B_2O_6 octahedral framework sub-structure and (b) $O'A_2$ tetrahedral framework sub-structure of the (c) ideal pyrochlore $O'A_2 \cdot B_2O_6$ or $A_2B_2O_7$ structure-type projected along a direction close to $\langle 110 \rangle$.

This displacive disorder (in particular, "… the local hopping of atoms in the O′ and *A* site positions among several local potential minima …" [16]) is commonly reported to be associated with anomalous low-temperature glass-like dielectric behaviour and, in particular, with a low-temperature peak in the dielectric loss which moves systematically to higher temperatures upon increasing frequency [16–19]. As this has the potential to rule out the use of such materials at microwave frequencies, it becomes very important to investigate the local crystal chemistry underlying this displacive disorder in order to obtain insight into its effect upon the dielectric properties of Bi-based pyrochlore systems. In recent papers, the observation of a characteristic, highly structured diffuse intensity distribution via electron diffraction and its interpretation in terms of highly correlated compositional and displacive disorder [19,20] has been used to make significant progress towards attaining this insight in the particular case of BZN and BZN-related pyrochlores.

In the case of the $Bi_2(M^{III}Nb^{V})O_7$ pyrochlore systems, however, the mechanism underlying displacive disorder appears to be distinctly different to that of BZN and BZN-related pyrochlores. The focus of the current paper is therefore upon the $Bi_2(M^{III}Nb^{V})O_7$, $M =$ In and Fe, pyrochlore systems and the interaction between their local crystal structure and dielectric properties. Electron diffraction is again used to search for evidence of correlated disorder. The effect upon structure as well as dielectric properties of partial substitution of the Bi^{3+} ions on the pyrochlore *A* sites with Y^{3+} ions is also investigated.

2. Experimental

Samples of nominal stoichiometry Bi_2FeNbO_7 (BFN), $Bi_{1.5}Y_{0.5}FeNbO_7$ (BYFN), Bi_2InNbO_7 (BIN), and $Bi_{1.5}Y_{0.5}InNbO_7$ (BYIN) were prepared by solid-state reaction via thoroughly mixing high purity Bi_2O_3 (Merck), Fe_2O_3 (Atomergic), Y_2O_3 (ROC/RIC), In_2O_3 (Merck) and Nb_2O_5 (Aldrich). The raw materials were dried at 120 °C for 24 h to remove adsorbed water before mixing. The resultant powders were then ground in an agate mortar under acetone for 30 min, pressed into pellets and then annealed at temperatures from 900 to 1100 °C for periods ranging from 2 to 48 h. The XRD and electron diffraction patterns of the samples annealed for 2 and 48 h did not differ significantly. Taking into consideration the crystallizability and density of samples, the optimized final annealing process was determined to be 1000 °C for 2 h for BFN, 1050 °C for 2 h for BYFN, and 1100 °C for 48 h for the In-containing samples.

All the resultant annealed samples were found to be quite dense (important for dielectric properties measurements). The measured density of the Bi_2FeNbO_7 sample, for example, was 7.65 g/cm^3, corresponding to 99% of theoretical density while that of Bi_2InNbO_7 was 7.80 g/cm^3, corresponding to 97% of theoretical density. Both sides of the resultant pellets were also polished and then brushed with silver conductive paste followed by heat treatment at 550 °C for 30 min in order to ensure good electrical contact. Frequency-dependent dielectric spectra were then collected at room temperature using a high precision LCR meter (Agilent 4284A) from 40 Hz to 1 MHz.

XRD data were collected using a Guinier–Hägg camera with CuKα_1 radiation to determine phase purity. Silicon

(NBS No. 640) was added as an internal standard for accurate determination of the unit cell. TEM investigation was carried out in a Philips EM 430 TEM on crushed grains of the samples dispersed onto holey carbon-coated copper grids.

Elemental analyses in the case of the BFN sample were performed at 15 kV and 1 nA on a JEOL 6400 scanning electron microscope (SEM) using electron probe micro-analysis (EPMA) in back-scattered geometry. Samples were prepared by mounting the powders in resin, polishing to a $<1\,\mu m$ finish followed by the application of a thin carbon coat using pure Fe, NbO_2F and Bi_2Se_3 as compositional standards.

3. Results

3.1. XRD results

The average structures of all samples were determined by powder XRD to be cubic with the expected ideal pyrochlore space group symmetry of $Fd\bar{3}m$. The cubic unit cell parameters, refined from Guinier XRD data using the UnitCell program [21], are 10.5255(1) Å for BFN, 10.4430(1) Å for BYFN, 10.7917(1) Å for BIN, and 10.6951(1) Å for BYIN. In the case of the BFN sample, a few weak additional lines were observed which did not fit to the majority cubic pyrochlore phase. EPMA was thus carried out to determine the composition of the dominant pyrochlore phase.

3.2. EPMA results

Using pure Fe, NbO_2F and Bi_2Se_3 as standards, the composition of the dominant cubic pyrochlore phase in the nominal Bi_2FeNbO_7 sample was found to be homogeneous from grain to grain and of average stoichiometry $Bi_{1.96(3)}Fe_{1.14(1)}Nb_{0.90(1)}O_{6.90}$ from five separate spot analyses. The composition has been normalized assuming four metal ions. A very recent much more detailed phase analysis investigation of the Bi_2O_3–Fe_2O_3–Nb_2O_5 system, however, suggest that our standards have led to a slight systematic over-estimation of the Bi content and a slight under-estimate of the Nb content and that a more accurate composition for our sample should be $Bi_{1.84}Fe_{1.20}Nb_{0.96}O_{6.97}$ [22]. This has since been confirmed by synthesis of a single-phase sample at this composition. Using this sample as a standard, the composition of the dominant cubic pyrochlore phase in our initial sample then was analyzed as $Bi_{1.89(3)}Fe_{1.16(1)}Nb_{0.95(1)}O_{6.95}$.

3.3. Electron diffraction results

In a recent diffraction investigation of Bi_2InNbO_7 [14], we reported preliminary electron diffraction evidence for β-cristobalite-type orientational disorder (see Fig. 2) of the $O'Bi_4$ tetrahedra that make up the $O'A_2$ sub-structure of the ideal pyrochlore structure type. Note that the lack of

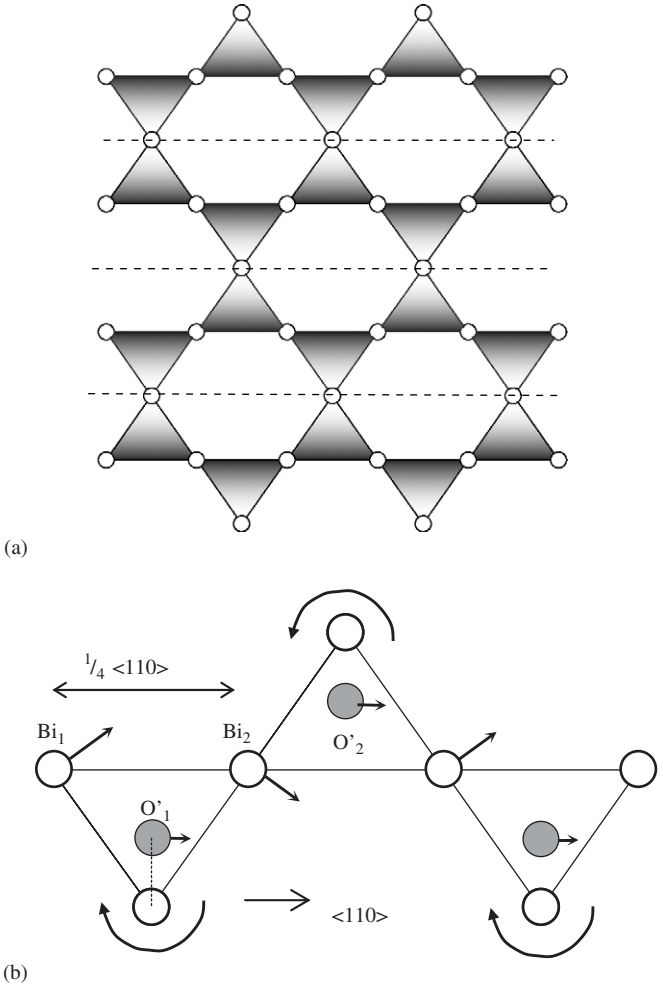

Fig. 2. The characteristic β-cristobalite-type displacive disorder (b) of the $O'Bi_2$ sub-structure (a) of the ideal pyrochlore structure type of Bi-pyrochlores. Note that rotation of any one $O'Bi_4$ tetrahedron around the appropriate $\langle 1\bar{1}0\rangle$ tetrahedral edge automatically constrains all the tetrahedra in that particular $\langle 110\rangle$ column to rotate as shown in (b) but does not constrain the sense of tetrahedral rotation from one such $\langle 110\rangle$ column to the next. The individual $\langle 110\rangle$ columns are delineated by the dashed lines in (a).

correlation in the sense of this tetrahedral edge rotation from one $\langle 110\rangle$ column to the next (across the dashed lines in Fig. 2a) ensures that such displacive shifts give rise only to structured diffuse scattering rather than additional satellite reflections. The characteristic diffraction signature of displacive disorder of this type is the existence of a highly structured, diffuse intensity distribution in the form of transverse polarized, $\{1\,1\,0\}^*$ sheets of diffuse intensity, perpendicular to each of the six $\langle 110\rangle$ directions of real space [23,24]. That a closely related such diffuse intensity distribution is characteristic not only of Bi_2InNbO_7 but also of $Bi_{1.89}Fe_{1.16}Nb_{0.95}O_{6.95}$ is apparent from the following electron diffraction results.

Fig. 3, for example, shows (a) $\langle 11\bar{2}\rangle$, (b) $\langle 22\bar{3}\rangle$, (c) $\langle 33\bar{4}\rangle$ and (d) close to $\langle 11\bar{1}\rangle$ zone axis electron diffraction patterns (EDPs) typical of $Bi_{1.89}Fe_{1.16}Nb_{0.95}O_{6.95}$. Such EDPs were quite reproducible from grain to grain. Notice

the presence of characteristic polarized diffuse streaking running through selected parent Bragg reflections, **G**, along three separate reciprocal space directions in each of *a*,*b*,*c* and *d*. In each case, the direction of this diffuse streaking is perpendicular to a particular $\langle 110 \rangle$ direction of real space. In Fig. 3b, for example, diffuse streaking occurs running through particular parent Bragg reflections along the $[668]^*(= [244]^* + [424]^*)$, $[10, \bar{4}, 4]^*(= [424]^* + 3[2\bar{2}0]^*)$ and $[\bar{4}, 10, 4]^*(= [244]^* - 3[22\bar{2}]^*)$ directions of reciprocal space, perpendicular to the [100], [011] and [101] real space directions, respectively. The continued presence of diffuse streaking of this type despite the changing incident beam orientation from *a* to *b* to *c* to *d* shows that the streaking is not localized to that particular reciprocal space direction but rather forms part of $\{110\}^*$ sheets of diffuse intensity in reciprocal space perpendicular to each of the $\langle 110 \rangle$ directions of real space.

Note furthermore that there are 'extinction conditions' associated with this diffuse streaking, e.g., the diffuse streaking along the $[668]^*$ direction in Fig. 3b runs through the $[hkl]^*$, $h-k = 4J$, J an integer, parent Bragg reflections such as, e.g. $[2\bar{2}0]^*$ but not through reflections such as $[424]^*$, etc. Likewise the diffuse streaking running along the $[10, \bar{4}, 4]^*$ direction runs through the $[hkl]^*$, $k+l = 4J$, J an integer, parent Bragg reflections such as $[244]^*$ but not through reflections such as $[424]^*$, etc. Such characteristic pseudo-extinction conditions are characteristic of β-cristobalite-type orientational disorder of the $O'Bi_4$ tetrahedra that make up the $O'A_2$ sub-structure of the ideal pyrochlore structure type and arise because of the correlated displacement of heavily scattering Bi ions separated by 1/4 $\langle 110 \rangle$ (see, for example, Fig. 2b and Eq. (4) of Ref. [25] for the theoretical details).

Notice also that virtual 'satellite reflections' in the form of quite distinct "peaks" in diffuse intensity (arrowed in Fig. 3) arise whenever the three diffuse streaks perpendicular to the $\langle 110 \rangle$ intersect, e.g., at $\mathbf{G} \pm \frac{1}{2}[3\bar{1}1]^* \equiv \mathbf{G}' \pm \frac{1}{2}[\bar{1}\bar{1}1]^*$ in Fig. 3a, at $\mathbf{G} \pm (2J/7)[668]^* \equiv \mathbf{G}' \pm (2J/7)[\bar{1}\bar{1}1]^*$ in Fig. 3b, at $\mathbf{G} \pm (2J/5)[446]^* \equiv \mathbf{G}' \pm (2J/5)[\bar{1}\bar{1}1]^*$ in Fig. 3c and at $\mathbf{G} \pm \frac{1}{3}\langle 224 \rangle^* \equiv \mathbf{G}' \pm \frac{1}{3}[\bar{1}\bar{1}1]^*$ in Fig. 3d (J an integer). The fact that such peaks in the diffuse intensity continue to arise regardless of orientation confirms that they form part of essentially continuous 1-D rods of diffuse intensity running along the $\mathbf{G} \pm \varepsilon \langle 111 \rangle^*$ directions of

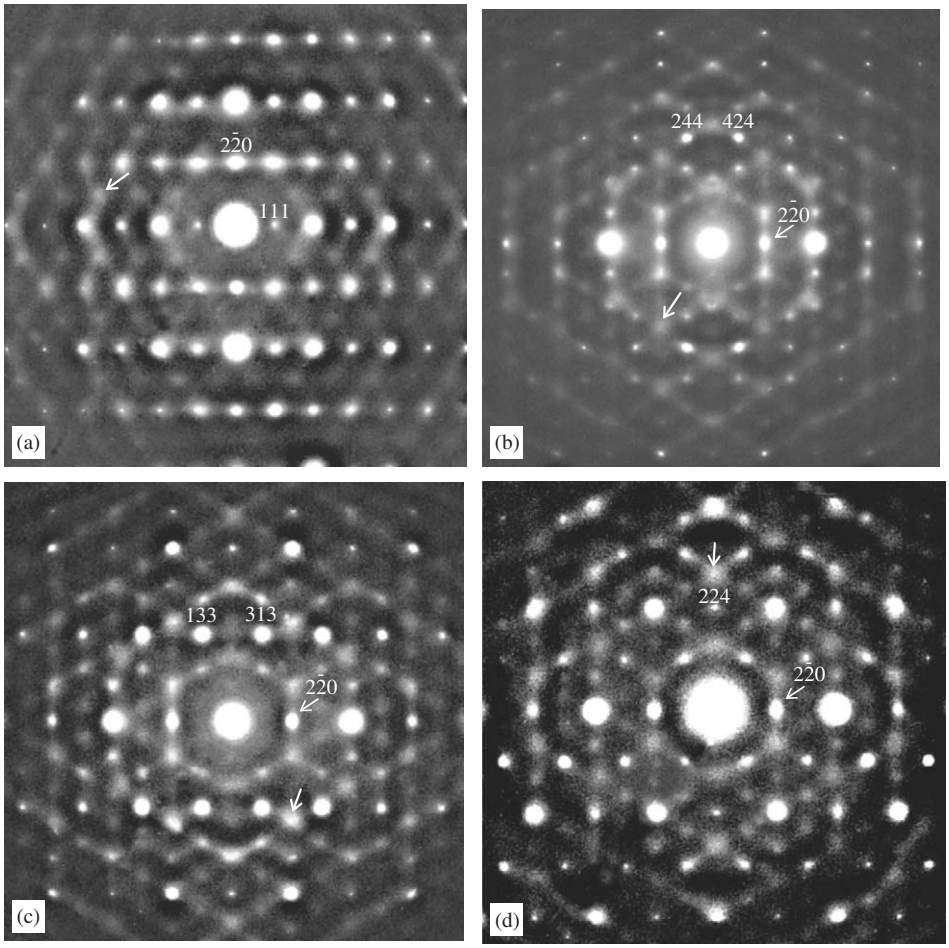

Fig. 3. Typical (a) $\langle 11\bar{2} \rangle$, (b) $\langle 22\bar{3} \rangle$, (c) $\langle 33\bar{4} \rangle$ and (d) close to $\langle 11\bar{1} \rangle$ zone axis electron diffraction patterns (EDPs) of BFN. Note the presence of characteristic polarized diffuse streaking running through selected parent Bragg reflections, **G**, along three separate reciprocal space directions in each of *a*, *b*, *c* and *d*. In each case, the direction of this diffuse streaking is perpendicular to a particular $\langle 110 \rangle$ direction of real space.

reciprocal space. Such diffuse rods imply the existence of correlated {1 1 1} planes of Bi displacements that are uncorrelated from one such {1 1 1} plane to the next.

Finally notice that the 'extinction conditions' characteristic of the {110}* sheets of diffuse intensity are also characteristic of the $\langle 111 \rangle^*$ rods of diffuse intensity, e.g., the $\mathbf{G} \pm 2J/7$ [668]* peaks in the diffuse intensity in Fig. 3b only run through parent Bragg reflections for which $h-k$, $k+l$ and $h+l$ all equal $4J$, J an integer. Clearly the displacive disorder responsible for these $\langle 111 \rangle^*$ rods of diffuse intensity arises from an appropriate linear combination of tetrahedral edge rotations of the type shown in Fig. 2b involving Bi displacements along the three $\langle 1\bar{1}0 \rangle$ real space directions perpendicular to the particular $\langle 111 \rangle^*$ rod of diffuse intensity and leading to resultant tetrahedral rotation around the $\langle 111 \rangle$ axis (as shown in Fig. 4a). Note that there need be no correlation in the sense of tetrahedral rotation from one such {111} plane to the next as required by the experimentally observed rods of diffuse intensity.

In the case of BIN, weak diffuse streaking perpendicular to the six $\langle 110 \rangle$ directions is again apparent (see e.g., Fig. 4 of [14]) as well as the presence of diffuse rods running along the $\langle 111 \rangle^*$ reciprocal space directions. Fig. 5, for example, shows (a) $\langle 12\bar{3} \rangle$ and (b) $\langle 11\bar{2} \rangle$ zone axis EDPs of BIN. Weak polarized diffuse streaking running along $\langle 5\bar{1}1 \rangle^*$ and $\langle 2\bar{4}2 \rangle^*$, for example, is apparent in Fig. 5a as well as the presence of quite strong peaks in the diffuse intensity (arrowed) at the $\mathbf{G} \pm \frac{1}{3}\langle 5\bar{1}1 \rangle^* \equiv \mathbf{G}' \pm \frac{1}{3}[\bar{1}\bar{1}1]^*$ positions of reciprocal space. Likewise, strong peaks in the diffuse intensity occur at the $\mathbf{G} \pm \frac{1}{2}\langle 3\bar{1}1 \rangle * \equiv \mathbf{G}' \pm \frac{1}{2}[\bar{1}\bar{1}1]^*$ positions of reciprocal space in Fig. 5b. In the case of BIN, it appears that the $\langle 111 \rangle^*$ rods of diffuse intensity are rather stronger in intensity than the {110}* sheets of diffuse intensity, i.e., the displacive disorder of the Bi ions is predominantly of the type shown in Fig. 4a rather than that shown in Fig. 2b.

Clearly the "hopping" (displacive disorder) of the Bi and O′ ions within the O′Bi_2 sub-structure of both BIN and $Bi_{1.89(3)}Fe_{1.16(1)}Nb_{0.95(1)}O_{6.95}$ is highly correlated and not at all independent of one another. Given that the low-temperature dielectric loss properties of Bi-pyrochlores has been associated with such "hopping", the effect of compositional disorder on the pyrochlore A sites has also been investigated by the replacement of 25% of the Bi ions on the pyrochlore A site with Y^{3+} ions to see what effect such a substitution might have on both the diffraction and dielectric properties of the resultant BYFN and BIYN materials.

From the diffraction point of view, the effect of such A site substitution appears to be relatively small in that the highly structured diffuse intensity distribution characteristic of both BIN and BFN is also maintained in the case of the 25% Y substituted derivative compounds BYIN and BYFN, cf., e.g., the $[11\bar{1}]$ zone axis EDP of BYIN shown in Fig. 6a with that of BFN shown in Fig. 3d. Likewise, cf. the $\langle 11\bar{2} \rangle$ close to zone axis EDP of BYFN shown in Fig. 6b with that of BFN shown in Fig. 3a. The 1-D rods of diffuse intensity running along the $\mathbf{G} \pm \varepsilon \langle 111 \rangle^*$ directions of reciprocal space in the case of the BIN and BFN samples

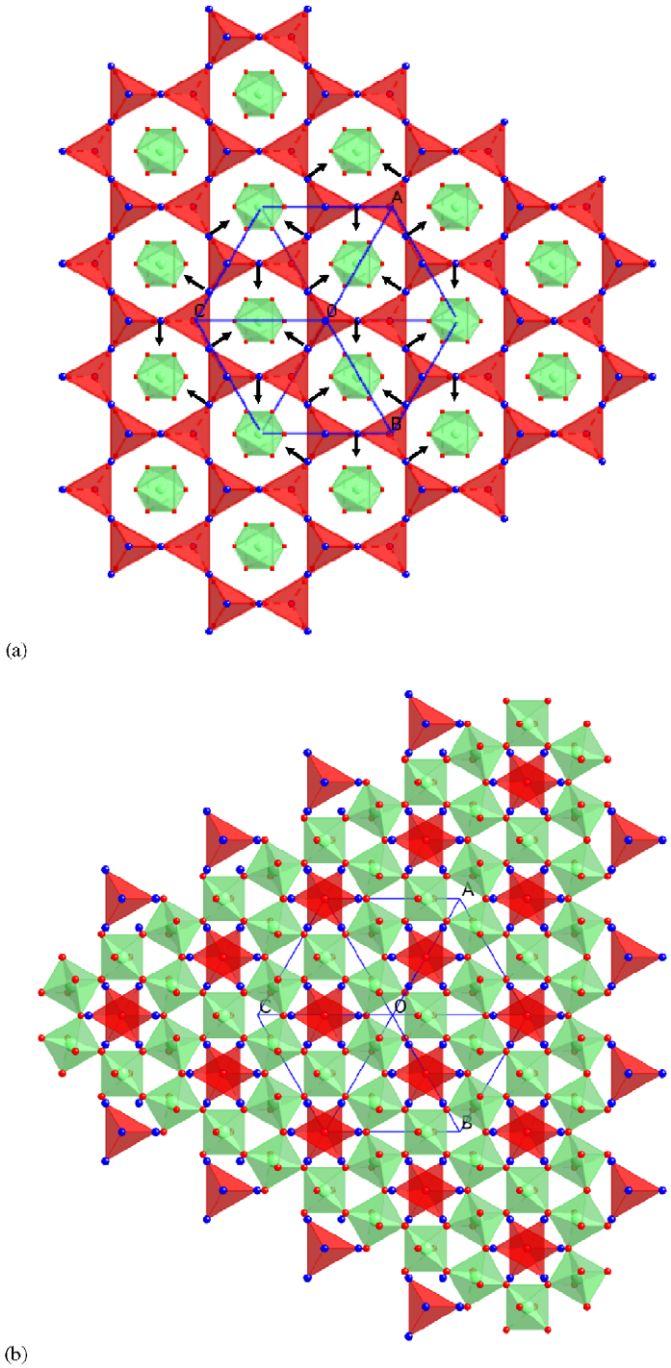

Fig. 4. (a) The pattern of correlated O′Bi_4 tetrahedral rotation around the $\langle 111 \rangle$ axis responsible for the observed $\langle 111 \rangle^*$ rods of diffuse intensity. There are two distinct types of {111} planes per primitive parent unit cell. These are shown in (a) and (b), respectively. Note that rotation of any O′Bi_4 tetrahedron around $\langle 111 \rangle$ automatically constrains all the tetrahedra in that particular $\langle 111 \rangle$ plane to rotate as shown in (a) but does not constrain the sense of tetrahedral rotation from one such $\langle 111 \rangle$ plane to the next. Note that each Bi ion moves essentially directly towards two of the O anions bonded to the B cations and directly away from two others.

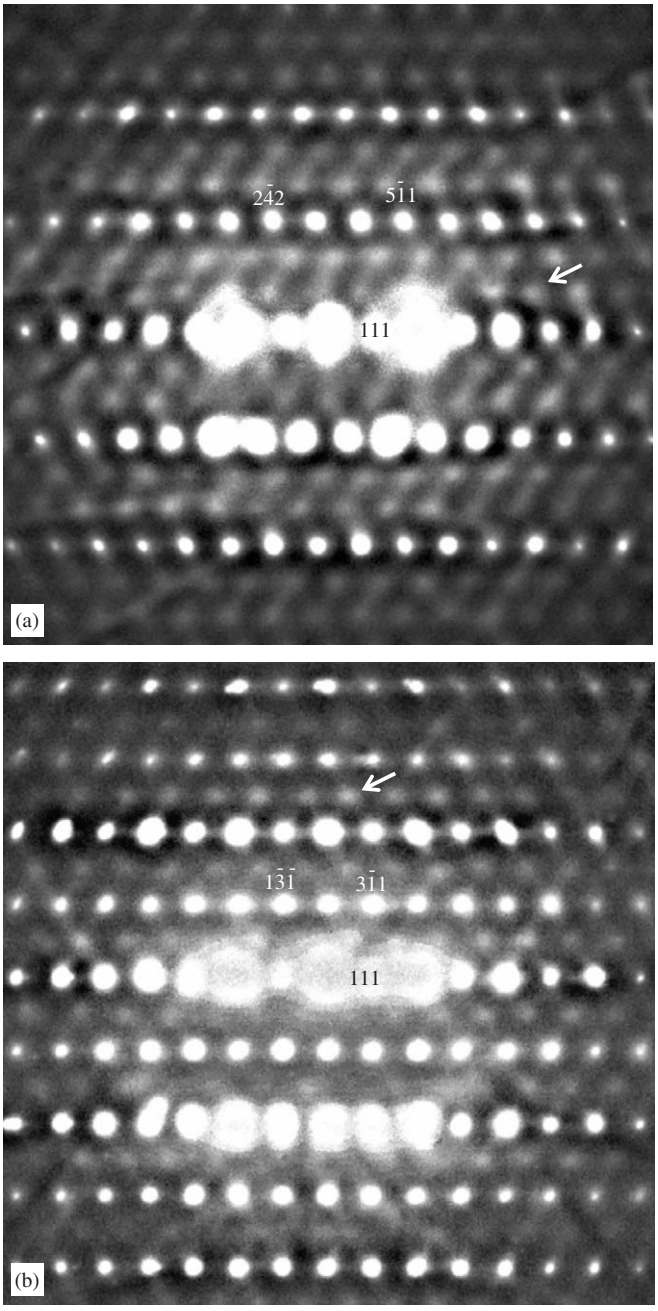

Fig. 5. Shows (a) $\langle 12\bar{3}\rangle$ and (b) $\langle 11\bar{2}\rangle$ zone axis EDPs typical of BIN. Notice the presence of quite strong diffuse blobs of intensity (arrowed) at the $\mathbf{G} \pm \frac{1}{3}[5\bar{1}1]^* \equiv \mathbf{G}' \pm \frac{1}{3}[\bar{1}\bar{1}1]^*$ positions of reciprocal space in (a) as well as at the $\mathbf{G} \pm \frac{1}{2}[3\bar{1}1]* \equiv \mathbf{G}' \pm \frac{1}{2}[\bar{1}\bar{1}1]*$ positions of reciprocal space in (b).

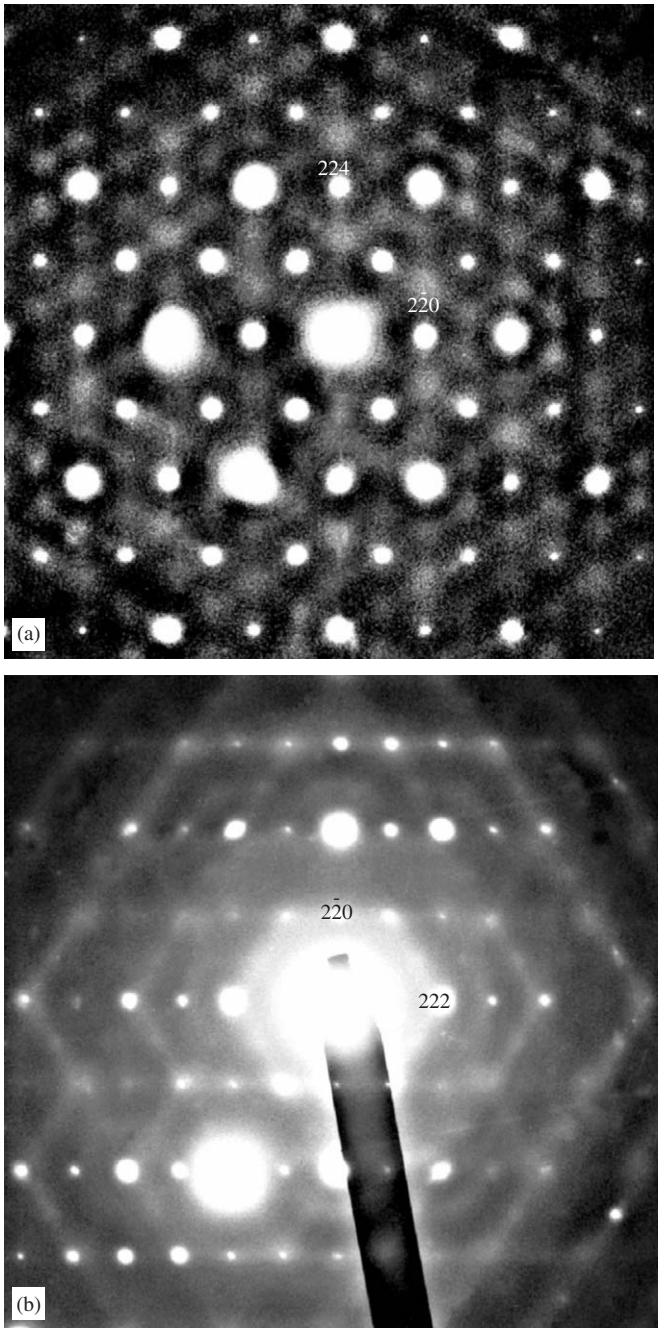

Fig. 6. Shows (a) a $[11\bar{1}]$ zone axis EDP of BYIN and (b) a close to $\langle 11\bar{2}\rangle$ zone axis EDP of BYFN. Note that the characteristic diffuse streaking perpendicular to $\langle 110\rangle$ directions of real space is clearly apparent in both samples.

appear to be reduced in the case of the BYFN and BYIN samples, particularly in the case of the BYFN sample.

3.4. Dielectric properties results

Fig. 7 shows the measured dielectric spectra for each of these four pyrochlore-type compounds. Both BFN and BIN were found to be good dielectric materials, indeed comparable with BZN and $Bi_2Zn_{2/3}Nb_{4/3}O_7$ [4]. The dielectric constant of BFN, for example, was found to be 100 while its dielectric loss was found to be 0.007 when measured at a frequency of 1 MHz at room temperature. For BIN, the corresponding numbers are 133 and 0.002, respectively. In the case of BIN, this is in good agreement with a previous result obtained by Cann et al. [7].

The measured high dielectric constant and low dielectric loss of BIN was found to be essentially frequency independent over the measured frequency range (from 40 Hz to 1 MHz). The dielectric constant as well as the dielectric loss of the BFN slowly but continuously decreased with increasing frequency. The dielectric constant

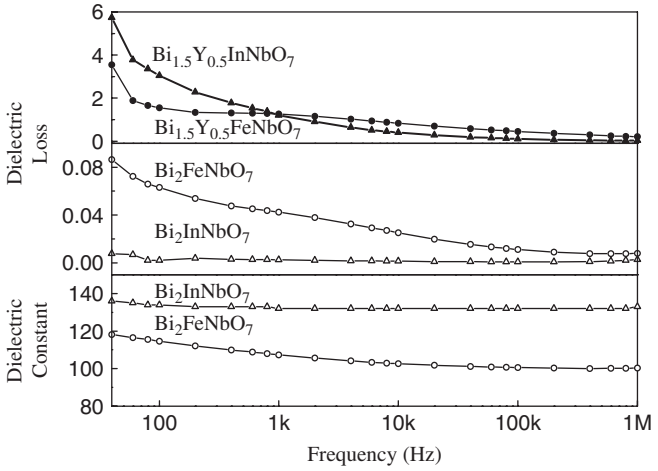

Fig. 7. Shows the measured dielectric spectra for each of BIN, BFN, BYIN and BYFN as a function of frequency from 40 Hz to 1 MHz. Note that the dielectric loss of both BIN and BFN increases dramatically (particularly at low frequency) when 25% of the Bi ions are substituted by Y as for BYIN and BYFN. Both BFN and BIN were found to be good dielectric materials with relatively high dielectric constants and relatively low dielectric losses, particularly in the case of BIN.

of BFN, while reduced at 1 MHz, nonetheless remained respectably high. These excellent dielectric properties, when combined with the known semiconductor properties of these materials, suggests that they have the potential to become new tuneable microwave dielectric materials. Furthermore, detailed investigation of the dielectric properties of these materials is in progress.

When the *A* site Bi ions were partially substituted by yttrium, the dielectric loss of both BYFN and BYIN immediately became very high, especially in the low-frequency range. The dielectric loss in both cases decreased with increasing frequency to values of 0.207 for BYFN and 0.026 for BYIN at 1 MHz. The latter is small enough to measure a corresponding dielectric constant which was 32 at 1 MHz. The obtained results suggest that both doped compounds have become semiconductors at room temperature. High dielectric losses in the low-frequency range suggests a large number of non-intrinsic defects contributing to electronic conductivity in these compounds. The question is why does substitution on the pyrochlore *A* site have such a strong effect on the dielectric properties of BIN and BFN? and why are $Bi_2M^{III}Nb^{V}O_7$ pyrochlores of this type necessarily displacively disordered?

4. Crystal chemistry

In order to attempt to answer these questions, insight is needed into the crystal chemistry underlying the observed diffuse distribution/s. We begin with a bond valence sum analysis of the average $Fd\bar{3}m$ pyrochlore (Bi on *16d* at 1/2, 1/2, 1/2; In/Fe/Nb on 16*c* at 000; O on 48*f* at *x*, 1/8, 1/8 and O′ on *8b* at 3/8, 3/8, 3/8; origin choice 2) structures of Bi_2InNbO_7 and $Bi_{1.89}Fe_{1.16}Nb_{0.95}O_{6.95}$ (for the purposes of this exercise we ignore the ~6% of Fe^{3+} on the pyrochlore *A* site for the latter sample) using the bond valence parameters ($R_0's$) of Brese and O'Keeffe [26]. For the purposes of this discussion, the ideal cubic pyrochlore structure type is described in terms of two intergrown component sub-structures—a B_2O_6 octahedral corner-connected sub-structure (see Fig. 1a) and an $O'A_2$ tetrahedral corner-connected sub-structure of anti-cristobalite structure type (see Fig. 1b). Note, however, that these two component sub-structures are by no means independent of one another in that the *A* cations of the latter are bonded reasonably strongly to the O anions of the former. Nonetheless, breaking the ideal cubic pyrochlore structure up in this way is a valid and useful means of investigating the local crystal chemistry of the overall structure.

4.1. The B_2O_6 octahedral sub-structure

Consider firstly the B_2O_6 octahedral corner-connected sub-structure (see Fig. 1a). The *B* cations in this sub-structure are each octahedrally co-ordinated by, and bonded to, six O anions at an average distance $R(B\text{–O}) = \sqrt{\{(x-1/4)^2 + 2\ (1/8)^2\}} \times a$ Å, dependent on the one unknown fractional co-ordinate of the ideal pyrochlore structure type, the *x* fractional co-ordinate of the O ion, as well as the cubic lattice parameter *a* (10.7917 Å in the case of Bi_2InNbO_7 and 10.5255 Å in the case of $Bi_{1.89}Fe_{1.16}Nb_{0.95}O_{6.95}$. For Nb^{5+} in the *B* site, the ideal *B*–O distance *R*(Nb–O) is given by that distance which corresponds to an apparent valence (AV) (see [26]) of 5/6. From [25], this distance is given by $1.911 - 0.37 \ln(5/6) = 1.9785$ Å. For In^{3+} or Fe^{3+} in the same *B* site, the equivalent ideal *B*–O distance $R(B\text{–O}) = 2.1585$ and 2.0155 Å, respectively, again using the R_0 parameters listed in [26]. Note that the ideal, or expected, B^{3+}–O^{2-} bond length is rather better matched to the ideal Nb^{5+}–O^{2-} bond length in the case of $B^{3+} = Fe^{3+}$ than in the case of $B^{3+} = In^{3+}$. Given that the average occupancy of the *B* site is $In_{1/2}Nb_{1/2}$ in the case of Bi_2InNbO_7 and $Fe_{0.525}Nb_{0.475}$ in the case of $Bi_{1.89}Fe_{1.16}Nb_{0.95}O_{6.95}$, the expected average *B*–O bond length, *R*(*B*–O) should then be 2.0685 and 1.9979 Å, respectively. The extent of local expansion/contraction of the BO_6 octahedra dependent upon the In^{3+}/Nb^{5+} or Fe^{3+}/Nb^{5+} distribution on the *B* sites should therefore be quite small for $B^{3+} = Fe^{3+}$ ($\sim \pm 0.02$ Å) and somewhat larger ($\sim \pm 0.09$ Å) for $B^{3+} = In^{3+}$.

An average *R*(*B*–O) bond length of 2.0685/1.9979 Å occurs for $x = 0.324/0.319$ given the relation between $R(B\text{–O}) = \sqrt{\{(x-1/4)^2 + 2\ (1/8)^2\}} \times a$ and *x*. The bond valence sum prediction for the value of *x* is thus 0.324 in the case of Bi_2InNbO_7 and 0.319 in the case of Bi_2FeNbO_7. Experimentally, *x* refined to 0.350 for Bi_2InNbO_7 when the disorder on the $O'Bi_2$ sub-structure (in particular, the disorder on the Bi site) was not taken into account and 0.325 when it was (see Table 1 of [14]). The latter makes crystal chemical commonsense in that the In^{3+} ion is then over-bonded in percentage terms by approximately the

Table 1
Calculated bond valence sums or apparent valences (AVs) for BIN and BFN using $x = 0.325$, $a = 10.7917$ Å for Bi_2InNbO_7 and $x = 0.319$, $a = 10.5255$ Å for Bi_2FeNbO_7.

$A = Bi^{3+}$	$B = In^{3+}$ or Nb^{5+}	AV(Bi)	AV(B)	AV(O)	AV(O′)
Bi	In	2.265	3.769	1.665	2.077
Bi	Nb	2.265	3.862	1.696	2.077
$A = Bi^{3+}$	$B = Fe^{3+}$ or Nb^{5+}	AV(Bi)	AV(B)	AV(O)	AV(O′)
Bi	Fe	2.503	3.150	1.480	2.427
Bi	Nb	2.503	4.751	2.013	2.427

same amount that the Nb^{5+} ions are under-bonded by, as might be expected from the crystal chemical point of view.

The value $x = 0.325$ is thus used in the bond valence sum calculations shown in Table 1 and in the discussion below. There is to date no experimentally reported refinement of x for Bi_2FeNbO_7 so we have used $x = 0.319$ in Table 1. Note that the In^{3+} ions are then ~25.6% over-bonded in the B site of Bi_2InNbO_7 whereas the Nb^{5+} ions are ~22.8% under-bonded in the same site. Likewise the Fe^{3+} ions are ~5.0% over-bonded in the B site of Bi_2FeNbO_7 whereas the Nb^{5+} ions are ~5.0% under-bonded in the same site. Ideally then, each O ion (co-ordinated by, and bonded to, two Bi ions and two B site ions) would prefer to be bonded to one In^{3+} or Fe^{3+} ion and one Nb^{5+} ion. It could then locally move away from the over-bonded M^{3+} cation towards the under-bonded Nb^{5+} cation.

From the point of view of strain minimization, the most efficient means of achieving this would be for the cations centreing the BO_6 octahedra in each of the tetrahedron of BO_6 octahedra characteristic of the B_2O_6 sub-structure (see Fig. 1a) to have the average stoichiometry, i.e., Nb_2In_2 or $Nb_{1.9}Fe_{2.1}$. Four out of six of the O ions bonded to these B ions could then be simultaneously repelled from the In^{3+} or Fe^{3+} site and, as it were, absorbed by the neighbouring Nb^{5+} ion. Given this, the most likely co-ordination environment for an O ion is [Bi_2InNb] or [Bi_2FeNb] rather than [Bi_2Nb_2] or [Bi_2In_2]/[Bi_2Fe_2] (see Table 2). Under these conditions, the bond valence sum requirements of the B site cations can then be quite well satisfied. On the other hand, the corresponding AV of the O ion under these circumstances is 1.681 in the case of Bi_2InNbO_7 and 1.747 in the case of $Bi_{1.89}Fe_{1.16}Nb_{0.95}O_{6.95}$ (see Table 2). The O anions are thus significantly under-bonded in both cases. (Note that the Bi cations in the ideal pyrochlore 1/2, 1/2, 1/2 position are even more significantly under-bonded, in each case by approximately twice as much as the O anions—cf. Tables 1 and 2.)

As the B site cations are well-bonded in this scenario, the systematic under-bonding of the O anions can only be rectified by an increased bond valence contribution from the two surrounding Bi ions to which the O anions are also bonded. Given that the Bi ions are even more significantly under-bonded in the ideal pyrochlore A site positions (see Table 1), it is clear that there is a strong crystal chemical driving force for the Bi cations and the O anions to move closer together. At the same time, however, note that the O′ ion centreing the O′Bi_4 tetrahedra is somewhat over-bonded, particularly in the case of $Bi_{1.89}Fe_{1.16}Nb_{0.95}O_{6.95}$ (see Table 1). The question is: what sort of displacements are needed in order to rectify or at least significantly improve the poor local crystal chemistry of the ideal pyrochlore average structures, i.e., the significant under-bonding of the Bi and O ions as well as the over-bonding of the O′ ions.

Table 2
Calculated AVs for BIN and BFN dependent upon the local [Bi_2B_2] stoichiometry of the four cations surrounding each O anion (again using $x = 0.325$, $a = 10.7917$ Å for Bi_2InNbO_7 and $x = 0.319$, $a = 10.5255$ Å for Bi_2FeNbO_7)

$A = Bi^{3+}$	[Bi_2In_2]	[Bi_2Nb_2]	[Bi_2InNb]
AV(O)[Bi_2B_2]	1.665	1.696	1.681
$A = Bi^{3+}$	[Bi_2Fe_2]	[Bi_2Nb_2]	[Bi_2FeNb]
AV(O)[Bi_2B_2]	1.480	2.013	1.747

4.2. The O′A_2 anti-cristobalite tetrahedral sub-structure

Now consider the second O′Bi_2 tetrahedral corner-connected sub-structure of anti-cristobalite structure type (see Fig. 1b). The O′ anion in this sub-structure is initially tetrahedrally co-ordinated by four Bi cations at a distance $R(O'–Bi) = (\sqrt{3}/8)a$ determined solely by the cubic lattice parameter a. Note that it is over-bonded for both Bi_2InNbO_7 and $Bi_{1.89}Fe_{1.16}Nb_{0.95}O_{6.95}$, particularly in the latter case (see Table 1). The O′ anions are thus quite happy for the local O′–Bi bond lengths to be slightly expanded as would be achieved by large amplitude tetrahedral rotation of the type shown in either Fig. 2b or Fig. 4a.

On the other hand, the Bi^{3+} ions are quite under-bonded in both cases (see Table 1). While each Bi^{3+} ion needs to move closer to at least some of the six O anions bonded to it (thereby improving the significant under-bonding of both), it cannot in this process afford to lose much of the contribution to its AV arising from the two surrounding O′ ions to which it is also bonded. These crystal chemical requirements ensure that the Bi ions can only displace orthogonal to their local O′–Bi–O′ axis and that the O′Bi_4

tetrahedra must rotate and translate essentially as rigid units, as necessitated by the tetrahedral rotation patterns shown in Figs. 2b and 4a (and experimentally in the form of the transverse polarized {110} sheets, and ⟨111⟩* rods, of diffuse intensity apparent in the diffuse distributions shown in Figs. 3, 5 and 6).

In the case of single tetrahedral edge rotation as shown in Fig. 2b, the induced shift of the Bi ions is necessarily away from the centre of the surrounding ring of six O anions and essentially directed towards one particular O anion and away from another (see, e.g., Fig. 8). Note that this occurs in a correlated fashion in that each Bi ion moves simultaneously towards one O anion and away from another while each of these O anions has one Bi move towards it and one away from it (see Fig. 8b). Such tetrahedral edge rotation thus simultaneously moves towards rectifying the initial under-bonding of both the Bi cations and these O anions as well as the initial over-bonding of the O′ anions. Indeed, bond valence sum calculations show that an O′Bi_4 tetrahedral rotation amplitude of 8.05° and associated rigid body translation along ⟨110⟩ of 0.186 Å in the case of Bi_2FeNbO_7 (see Fig. 8b) simultaneously increases the AV of the Bi and O anions directly involved by ~0.33 valence units (v.u.s) while reducing the AV of the O′ anion by 0.15 v.u.s. Clearly tetrahedral edge rotation of the type shown in Fig. 8 is capable of significantly improving the initially poor local crystal chemistry.

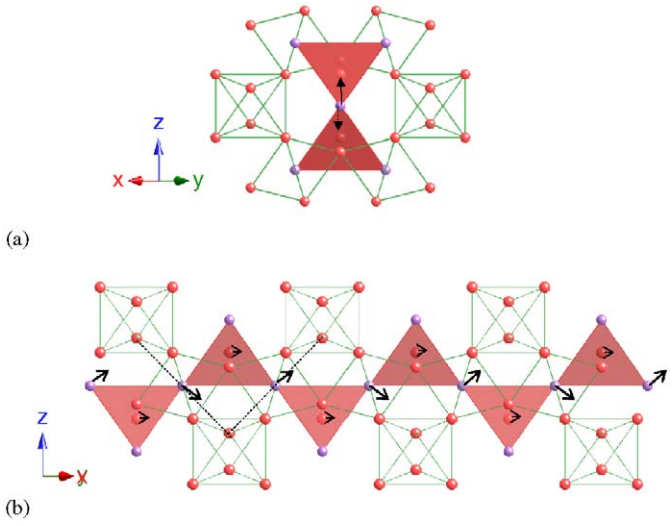

Fig. 8. Shows the characteristic β-cristobalite-type displacive disorder of the O′A_2 sub-structure (see Fig. 2) drawn relative to the surrounding B_2O_6 octahedral framework sub-structure. In (a) the tetrahedral edge rotation axes are in the plane whereas in (b) the tetrahedral edge rotation axes run along the projection direction.

On the other hand, the resultant increase in AV of the Bi ion is necessarily of very close to the same magnitude as the resultant increase for the O anion for single tetrahedral edge rotation as shown in Fig. 8. Given that the Bi cation is initially approximately twice as under-bonded as the O anion (see Tables 1 and 2), this is less than optimal. Tetrahedral edge rotation around ⟨111⟩ (as shown in Fig. 4a and resulting from a correlated linear combination of three appropriate single tetrahedral edge rotations), on the other hand, leads to an increase of the AV of the Bi cation which is necessarily ~twice as large as that of the O anions. This is as a result of the fact that each Bi ion moves simultaneously closer towards two O anions and further away from two other O anions while each O anion has one Bi ion move closer and one further away (see Fig. 4a). Bond valence sum calculations show that an O′Bi_4 tetrahedral rotation amplitude of 12.38° in the case of $Bi_{1.89}Fe_{1.16}Nb_{0.95}O_{6.95}$ (see Fig. 3a) increases the AV of the Bi ions by ~0.45–2.95 v.u.s, increases the AV of the O anions by ~0.29–2.04 v.u.s while reducing the AV of the O′ anion by 0.18–2.25 v.u.s. Clearly tetrahedral rotation of the type shown in Fig. 4 is even more capable of significantly improving the initial local crystal chemistry.

Experimentally, both ⟨111⟩* diffuse rods and {110}* diffuse sheets appear to coexist in the case of $Bi_{1.89}Fe_{1.16}Nb_{0.95}O_{6.95}$ (see Fig. 3). In the case of Bi_2InNbO_7, the balance appears to have shifted in the favour of ⟨111⟩* diffuse rods (see Fig. 5) while, in the case of the Y-doped samples, {110}* diffuse sheets appear to predominate (see Fig. 6). Bond valence sum calculations for the A site-doped BYIN and BYFN samples (see Tables 3 and 4) show that Y is even more under-bonded than Bi in the A site. This

Table 3
Calculated bond valence sums (AVs) for BYIN and BYFN using $x = 0.325$, $a = 10.6951$ Å for $Bi_{1.5}Y_{0.5}InNbO_7$ and $x = 0.319$, $a = 10.4430$ Å for $Bi_{1.5}Y_{0.5}FeNbO_7$

$A = Bi^{3+}$ or Y^{3+}	$B = In^{3+}$ or Nb^{5+}	AV(A)	AV(B)	AV(O)	AV(O′)
Bi	In	2.408	3.963	1.757	2.198
Bi	Nb	2.408	4.061	1.790	2.198
Y	In	1.940	3.963	1.673	1.771
Y	Nb	1.940	4.061	1.705	1.771
$A = Bi^{3+}$ or Y^{3+}	$B = Fe^{3+}$ or Nb^{5+}	AV(A)	AV(B)	AV(O)	AV(O′)
Bi	Fe	2.638	3.286	1.550	2.547
Bi	Nb	2.638	4.956	2.107	2.547
Y	Fe	2.125	3.286	1.462	2.052
Y	Nb	2.125	4.956	2.018	2.052

Table 4
Calculated AVs for BYIN and BYFN dependent upon the local $[A_2B_2]$ stoichiometry of the four cations surrounding each O anion (again using $x = 0.325$, $a = 10.6951$ Å for $Bi_{1.5}Y_{0.5}InNbO_7$ and $x = 0.319$, $a = 10.4430$ Å for $Bi_{1.5}Y_{0.5}FeNbO_7$)

$A = Bi^{3+}$ or Y^{3+}	$[B_2] = [In_2]$	$[B_2] = [Nb_2]$	$[B_2] = [InNb]$
AV(O)[Bi_2B_2]	1.757	1.790	1.774
AV(O)[Y_2B_2]	1.673	1.705	1.689
AV(O)[$BiYB_2$]	1.715	1.747	1.731
$A = Bi^{3+}$ or Fe^{3+}	$[B_2] = [Fe_2]$	$[B_2] = [Nb_2]$	$[B_2] = [FeNb]$
AV(O)[Bi_2B_2]	1.550	2.107	1.828
AV(O)[Y_2B_2]	1.462	2.018	1.740
AV(O)[$BiYB_2$]	1.506	2.062	1.784

accounts for the ~0.8% decrease in cubic cell parameter in each case upon substitution of 25% of the Bi sites by Y. Nevertheless the underlying crystal chemistry remains quite similar in that the *A* site ions as well as the O anions remain significantly under-bonded in the ideal pyrochlore positions necessitating tetrahedral edge rotation as shown in Fig. 2. It is difficult, however, to make further progress without full scale Monte Carlo disordered simulations, well beyond the scope of the current contribution.

5. Conclusions

Summarizing, it is clear that the large ADPs of Bi and O′ ions in average structure refinements of such Bi-pyrochlores (see, e.g., [14]) is directly related to the inherently poor local crystal chemistry of the ideal pyrochlore structure type (see Tables 1–4). The mechanism adopted for local structural distortion away from the ideal pyrochlore structure type is clearly tetrahedral edge rotation of the O′A_2 sub-structure, either of the individual type shown in Figs. 2 and 8 and/or of the correlated type (shown in Fig. 4). The inherent flexibility of the O′A_2 sub-structure and its relationship to the associated dielectric properties is, however, not so clear.

The much larger dielectric loss of BIN relative to BFN at low frequencies (see Fig. 7) suggests that the highly correlated ⟨111⟩ tetrahedral edge rotations of the type shown in Fig. 4a have intrinsically lower dielectric losses than Bi-pyrochlores for which the ⟨110⟩ tetrahedral edge rotations remain essentially independent of one another. In this context, it is worthwhile noting that single tetrahedral edge rotation of the type shown in Fig. 8b involves not only tetrahedral rotation but also rigid body translation of a nominally +4 charged O′Bi_2 column of tetrahedra along a ⟨110⟩ direction relative to the nominally −4 charged $M^{III}Nb^{V}O_6$ octahedral sub-structure. Reversal of the sense of rotation and hence rigid body translation of such columns of tetrahedra might well occur under the action of an applied electric field and hence provide a dielectric relaxation mechanism.

The reason for the significant deterioration in dielectric loss properties upon the substitution of 25% of the Bi ions in the pyrochlore *A* sites with Y ions is presumably related to the rather smaller electronegativity of the Y ions by comparison with that of the other constituent ions. *A* site disorder presumably also results in stronger local compositional and induced displacive disorder which experimentally dramatically increases dielectric losses as well as reducing the measured dielectric constants. High dielectric losses in the low-frequency range are usually taken as implying the existence of a large number of non-intrinsic defects contributing to electronic conductivity. Clearly doping has significantly degraded the dielectric properties of both BIN and BFN. Indeed, both doped compounds have become semiconductors at room temperature.

Acknowledgements

WS acknowledges financial support from the Department of Education, Science and Training (DEST) in the form of an Endeavour Australian Cheung Kong Award. YL, RLW, QZ and BJK acknowledge financial support from the Australian Research Council (ARC) in the form of ARC Discovery Grants. Discussions with T. Vanderah are greatly appreciated.

References

[1] W. Wersing, Curr. Opin. Solid State Mater. Sci. 1 (1996) 715–731.
[2] R.J. Cava, J. Mater. Chem. 11 (2001) 54–62.
[3] T.A. Vanderah, Science 298 (2002) 1182–1184.
[4] F. Zimmerman, M. Voigts, W. Menesklou, E. Ivers-Tiffée, J. Eur. Ceram. Soc. 24 (2004) 1729–1733.
[5] J.W. Lu, S. Stemmer, Appl. Phys. Lett. 83 (2003) 2411–2413.
[6] W. Ren, S. Trolier-McKinstry, C.A. Randall, T.R. Shrout, J. Appl. Phys. 89 (2001) 767–774.
[7] D.P. Cann, C.A. Randall, T.R. Shrout, Solid State Commun. 100 (1996) 529–534.
[8] X. Wang, H. Wang, X. Yao, J. Am. Ceram. Soc. 83 (2000) 147–153.
[9] M. Valant, P.K. Davies, J. Am. Ceram. Soc. 80 (1997) 2745–2748.
[10] A. Ismunandar, B.J. Kennedy, B.A. Hunter, T. Vogt, J. Solid State Chem. 131 (1997) 317–325.
[11] I. Radosavljevic, J.S.O. Evans, A.W. Sleight, J. Solid State Chem. 136 (1998) 63–66.
[12] M. Avdeev, M.K. Haas, J.D. Jorgensen, R.J. Cava, J. Solid State Chem. 169 (1997) 24–34.
[13] I. Levin, T.G. Amos, J.C. Nino, T.A. Vanderah, C.A. Randall, M.T. Lanagan, J. Solid State Chem. 168 (2002) 69–75.
[14] Q. Zhou, B.J. Kennedy, V. Ting, R.L. Withers, J. Solid State Chem. 178 (2005) 1575–1579.
[15] T.A. Vanderah, I. Levin, M.W. Lufaso, Eur. J. Inorg. Chem. 14 (2005) 2895–2901.
[16] S. Kamba, V. Porokhonsky, A. Pashkin, V. Bovtun, J. Petzelt, J.C. Nino, S. Trolier-McKinstry, M.T. Lanagan, C.A. Randall, Phys. Rev. B 66 (2002) 054106:1–054106:8.
[17] J.C. Nino, M.T. Lanagan, C.A. Randall, J. Appl. Phys. 89 (2001) 4512–4516.
[18] C. Ahn, Z. Yu, H.J. Youn, C.A. Randall, A.S. Bhalla, L.E. Cross, J. Nino, M. Lanagan, Appl. Phys. Lett. 80 (2002) 4807–4809.
[19] R.L. Withers, T.R. Welberry, A.-K. Larsson, Y. Liu, L. Norén, H. Rundlöf, F.J. Brink, J. Solid State Chem. 177 (2004) 231–244.

[20] Y. Liu, R.L. Withers, T.R. Welberry, H. Wang, H.L. Du, X. Yao, J. Electroceram. (2006) in press.
[21] B. Noläng, Inst. Materialkemi, Ångströmlaboratoriet, Box 538, SE-751 21, Uppsala, Sweden.
[22] M.W. Lufaso, T.A. Vanderah, I.M. Pazos, I. Levin, J.C. Nino, V. Provenzano, P.K. Shenck, R.S. Roth, J. Mater. Chem. (2006) in press.
[23] R.L. Withers, J.G. Thompson, T.R. Welberry, Phys. Chem. Miner. 16 (1989) 517–523.
[24] Y. Tabira, R.L. Withers, T. Yamada, N. Ishizawa, Z. Kristallogr. 216 (2001) 92–98.
[25] R.L. Withers, Z. Kristallogr. 220 (2005) 1027–1034.
[26] N.E. Brese, M.A. O'Keeffe, Acta Crystallogr. B 47 (1991) 192–197.